JACS
JOURNAL OF THE AMERICAN CHEMICAL SOCIETY
Article
pubs.acs.org/JACS

Basic Insights into Tunable Graphene Hydrogenation

Ricarda A. Schäfer, Daniela Dasler, Udo Mundloch, Frank Hauke, and Andreas Hirsch*

Department of Chemistry and Pharmacy and Joint Institute of Advanced Materials and Processes (ZMP), Friedrich-Alexander University of Erlangen-Nürnberg, Henkestrasse 42, 91054 Erlangen, Germany

Supporting Information

ABSTRACT: The hydrogenation and deuteration of graphite with potassium intercalation compounds as starting materials were investigated in depth. Characterization of the reaction products (hydrogenated and deuterated graphene) was carried out by thermogravimetric analysis coupled with mass spectrometry (TG-MS) and statistical Raman spectroscopy (SRS) and microscopy (SRM). The results reveal that the choice of the hydrogen/deuterium source, the nature of the graphite (used as starting material), the potassium concentration in the intercalation compound, and the choice of the solvent have a great impact on the reaction outcome. Furthermore, it was possible to prove that both mono- and few-layer hydrogenated/deuterated graphene can be produced.

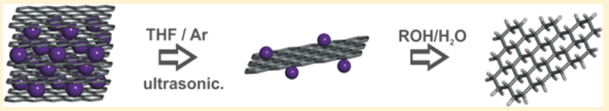

INTRODUCTION

The synthesis and complete characterization of fully hydrogenated graphene (graphane) remains to be a challenge in carbon allotrope chemistry.[1] Graphane has been theoretically studied by Sofo et al.[2] Recently, a variety of reports toward the synthesis of partially hydrogenated graphene have been published. These include the hydrogenation of graphene using hydrogen plasma[3] as well as wet chemical approaches.[4,5] In the latter case, the synthetic protocols are based on a Birch[6] type reduction sequence utilizing alcohols or water as proton sources. Liquid ammonia and alkali metals, like lithium or sodium, served as reducing agents. At the same time the reduction of graphite facilitates the exfoliation of the individual graphene sheets driven by the electrostatic repulsion of the charged layers. We have demonstrated that the application of water as proton source leads to very high degrees of hydrogenation, and the resulting stable reaction product shows a remarkable fluorescence behavior.[5,7] A critical drawback of this approach however is (a) the use of the somewhat difficult to handle liquid ammonia and (b) the restriction to control the degree of hydrogenation. We now introduce a new route toward hydrogenated graphene using potassium intercalated graphite as starting material and THF as inert solvent (Scheme 1). This reductive graphite activation procedure has already proven to be a versatile concept for the bulk synthesis of covalently functionalized graphene as the intermediate graphenides can be trapped by a variety of electrophiles like diazonium[8] or iodonium compounds[9] and alkyl or aryl iodides.[10,11] As a consequence, we have expected that reduced graphite intercalation compounds (GICs) are also suitable starting materials for subsequent protonations, leading to the formation of hydrogenated graphene. Since in GICs the degree of reduction can easily be controlled by the stoichiometry of the alkali metal, it should be possible to control the extent of hydrogenation, which is another advantage of this approach.

In order to study the general feasibility of the GIC protonation, we have systematically screened three different types of graphite—synthetic spherical (SGN18), natural flake (NG), and expanded powder (PEX10)—and varied (a) the amount of potassium and (b) the nature of the proton/deuteron source in order to obtain deeper insights into the underlying reactivity principles.

Scheme 1. Hydrogenation of Graphene Using Three Types of Graphite (Synthetic Spherical Graphite (SGN_{18}), Natural Flake Graphite (NG), and Expanded Powder Graphite (PEX10)) as Starting Material[a]

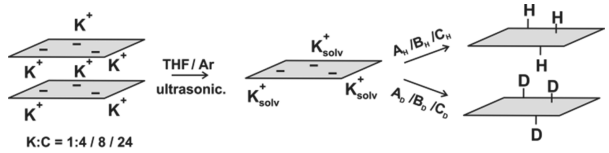

[a]In the initially generated potassium GICs the K:C ratio has been varied (K:C = 1:4, 1:8, and 1:24). Three different sources for protons (A_H = H_2O, B_H = MeOH, C_H = *t*-BuOH) and deuterons (A_D = D_2O, B_D = MeOD, C_D = *t*-BuOD) have been used.

The reaction products have been characterized in detail by statistical Raman spectroscopy (SRS) and microscopy (SRM) as well as thermogravimetric analysis coupled with mass spectrometry (TG-MS). Our results clearly show that in this way the bulk synthesis of hydrogenated graphene—with tunable hydrogen content (5%−66%)—can be accomplished. This approach provides a new, solution-based access tool for hydrogenated graphene with tailor-made hydrogen contents, starting from the ubiquitary available material graphite.

RESULTS AND DISCUSSION

In previous studies it has been noticed that the combination of KC_8 with proton sources leads to the formation of varying products ranging from nanoscrolls[12] to partly hydrated or

Received: November 16, 2015
Published: January 15, 2016

DOI: 10.1021/jacs.5b11994
J. Am. Chem. Soc. 2016, 138, 1647−1652

hydrogenated graphite depending on the reaction conditions.[13] We have recently shown that the ultrasound agitation of potassium intercalated graphite leads to an efficient exfoliation of the graphitic starting material and to the generation of negatively charged monolayer graphene.[8] The corresponding experimental setup has been adapted in the present study.

In particular, the potassium GIC (SGN18: spherical graphite; 18 μm flake size) has been exfoliated in THF via sonication, and subsequently the intermediately generated graphenide flakes have been trapped with 10 equiv of a hydrogen or deuterium source. The dispersion of the intercalate in THF via sonication marks the fundamental difference to previously reported approaches,[12−15] which were carried out without ultrasound agitation and in the most cases in the absence of any solvent. The Coulomb force driven exfoliation of graphite has a fundamental impact on the reaction mechanism and on the nature of the final product, since the efficient individualization of the packed graphene layers provides a huge and highly reactive surface area for the subsequent covalent functionalization. In analogy to other reductive functionalization sequences, a single-electron transfer from the charged graphenide sheets to the trapping water or alcohol should lead to the formation of hydrogen radicals.[13] Subsequently, these radicals can either recombine to molecular hydrogen or attack the extended sp^2-carbon lattice yielding hydrogenated graphene sheets. We suggest that due to the close proximity between the generated radicals and the graphene sheets the latter process (hydrogenation) is predominant.

In order to prove that the successful hydrogenation of graphene is possible, thermogravimetric analysis coupled with mass spectrometry (TG-MS) has been applied. For this purpose the samples were heated from rt to 700 °C under a constant flow of helium and the thermally detached entities were analyzed by an EI mass spectrometer. As exemplarily depicted in Figure 1 for $\mathbf{G_{1:4}C_H}$ (SGN18, GIC potassium concentration of K:C = 1:4 and *t*-BuOH as trapping reagent), two major steps of mass loss, namely region A: 220−380 °C and region B: 380−500 °C (indicated in red), can be identified. The first step can be attributed to molecular fragments exhibiting *m*/*z* 17/18/31 and 72 (Figure S1), which are due to residues of water, hydroxides, or THF that have been co-intercalated or encapsulated between the reaggregated graphene sheets. These findings are in total agreement with previously published results.[9]

In the second region B, the observed mass loss of 4.8% can directly be attributed to the dehydrogenation of the sample, as the mass spectrometric analysis exhibits a pronounced peak (60 pA intensity) for *m*/*z* 2 in this temperature range. Thus, we correlated the hydrogen mass loss with the residual carbon mass at 700 °C. This resulted in a degree of hydrogenation of 62.3% ($(C_1H_{0.6})_n$) (Table ST4). To ensure that the detected hydrogen is introduced by the alcohol trapping reagent, we substituted the hydrogen source with a deuterium source. TG-MS analysis of the sample $\mathbf{G_{1:4}C_D}$ has been carried out under a constant nitrogen flow, exhibiting a similar mass loss of 5.5% (Figure 2a). Simultaneously, the recorded molecular fragments with *m*/*z* 3 and 4 (Figure 2b and Figure S2) can be attributed to DH and D_2 with a maximum ion current at the same temperature as measured for $\mathbf{G_{1:4}C_H}$. The degree of deuteration of 42.4% ($(C_1D_{0.4})_n$) was calculated according to the calculation of the degree of hydrogenation (Table ST4).

Thus, it can be concluded that the hydrogen or the deuterium is directly introduced by the addition of the respective trapping reagent. It is most likely that the appearance of HD can be traced back to hydrogen exchange reactions with the residual H_2O traces (trapped between the individual graphene galleries) in the pristine graphite.

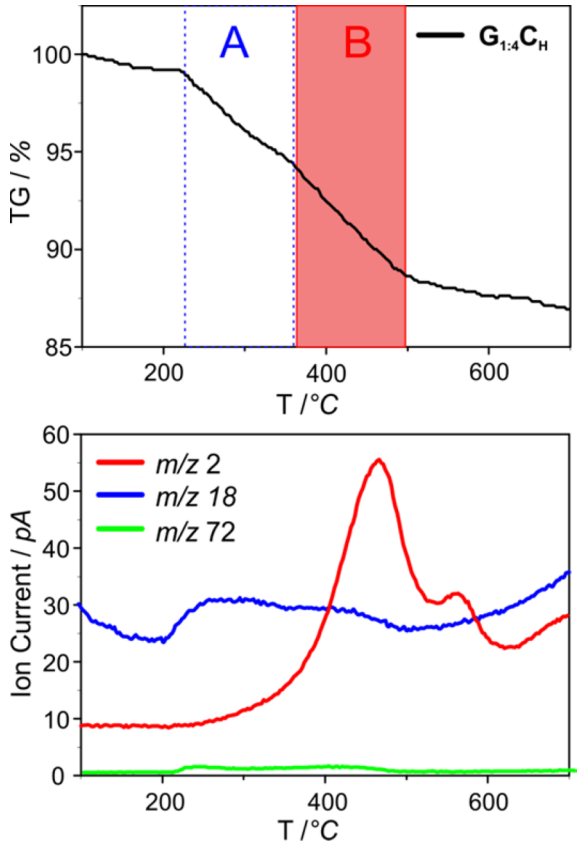

Figure 1. Top: TG profile of hydrogenated graphene $\mathbf{G_{1:4}C_H}$ (SGN18) with region A and B. Bottom: MS trace for *m*/*z* 2 (H_2), 18 (H_2O), and 72 (THF).

For a deeper understanding of the influence of the deuterium source and for manifesting our proposed mechanism, we investigated three different systems, namely, *t*-BuOD, MeOD, and heavy water. The amount of deuteration can slightly be increased by the use of deuteriomethanol (6.1% mass loss in temperature region B, degree of deuteration: 48.5%, $(C_1D_{0.5})_n$) with respect to *t*-BuOD (5.5% mass loss, degree of deuteration: 42.4%, $(C_1D_{0.4})_n$) but drastically decreases when D_2O (2.2% mass loss, degree of deuteration: 15.4%, $(C_1D_{0.2})_n$) was applied as trapping reagent (Figure 2a,b and Table ST4). Interestingly, this reaction outcome is in contrast to the results obtained under classical Birch reduction conditions, where water yields hydrogenated graphene with the highest degree of functionalization.[5] This fact can be explained with the nature of the solvent. In the latter case, ammonia is used at −75 °C and interacts with the trapping water (formation of ammonium hydroxide in an equilibrium reaction).

Furthermore, the resulting reactivity order marks the difference between the Birch reduction and our reductive hydrogenation approach. In the Birch reduction solvated electrons are involved in the reduction mechanism, whereas in the reductive hydrogenation of potassium GIC starting materials the resulting graphenides can directly be traced back to the alkali metal intercalation process followed by the coulomb driven exfoliation of the charged sheets. The used KC_4 consists of $^1/_8$ more potassium than the highest ordered GIC of potassium KC_8. Thus, we suspect the potassium excess to aggregate on the

DOI: 10.1021/jacs.5b11994
J. Am. Chem. Soc. 2016, 138, 1647−1652

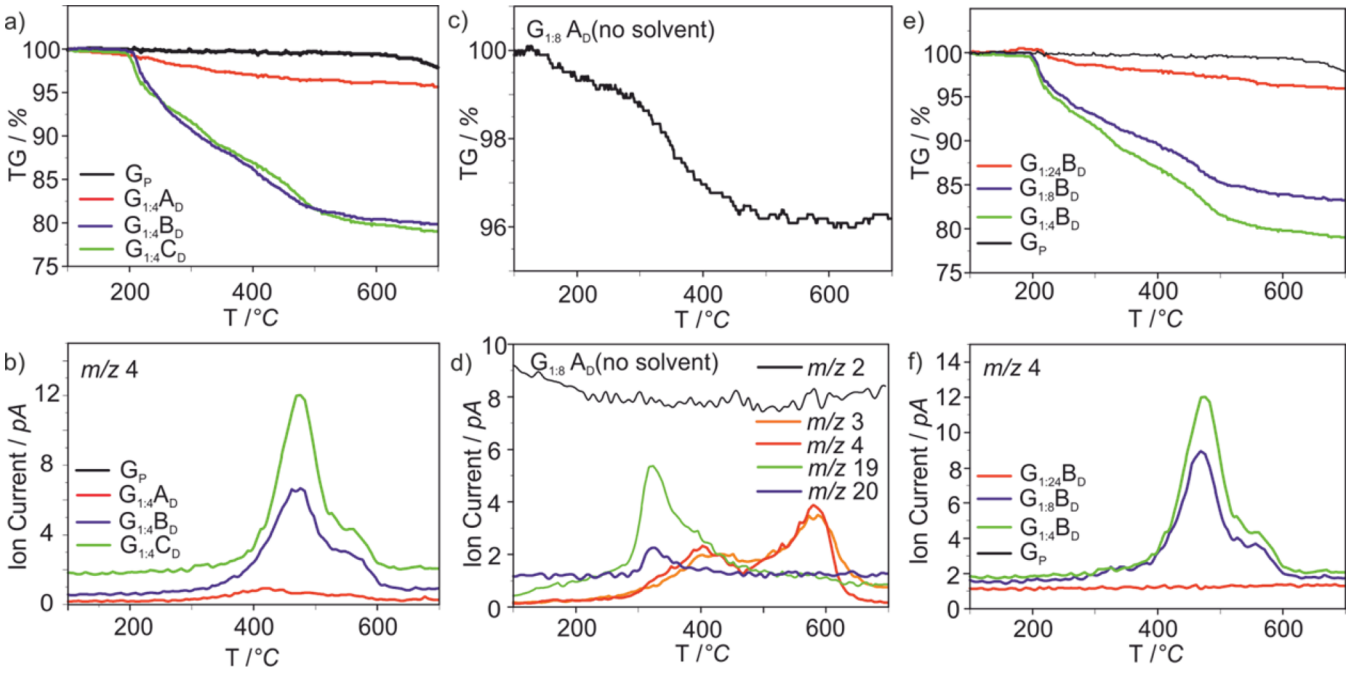

Figure 2. (a) TG profile of deuterated graphene $\mathbf{G_P}$, $\mathbf{G_{1:4}A_D}$, $\mathbf{G_{1:4}B_D}$, and $\mathbf{G_{1:4}C_D}$. (b) Corresponding MS traces for m/z 4 (D_2). (c) TG profile of $\mathbf{G_{1:4}A_D}$**(no solvent)**. (d) MS traces of $\mathbf{G_1}$**:**$_4$**AD(no solvent)** for m/z 2 (H_2), 3 (HD), 4(D_2), 19 (HDO), and 20 (D_2O). (e) TG profile of $\mathbf{G_{1:4}B_D}$, $\mathbf{G_{1:8}B_D}$, $\mathbf{G_{1:24}B_D}$, and $\mathbf{G_P}$. (f) MS traces for m/z 4(D_2) of $\mathbf{G_{1:4}B_D}$, $\mathbf{G_{1:8}B_D}$, and $\mathbf{G_{1:24}B_D}$.

graphene/graphite sheet surfaces. Since it is not part of the noncovalent interaction between negatively charged graphene layers and the potassium cation, it will react as elementary potassium. Elemental potassium is known to react vigorously with water to form hydrogen. Alcohols in contrast react slower with potassium and less exothermic which favors the hydrogenation of the graphene sheet instead of the formation of molecular hydrogen.

In order to further investigate the influence of the solvent system, we used liquid ammonia instead of THF for the exfoliation/dispersion of the potassium intercalation compound $\mathbf{G_{1:4}}$ and D_2O as trapping component (Scheme 2).

Scheme 2. Reaction of Spherical Graphite Intercalated with Potassium (K:C = 1:4)[a]

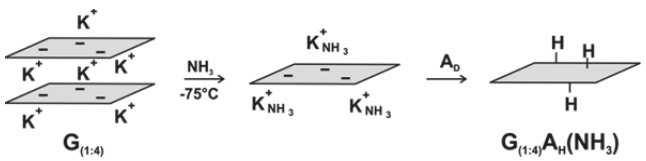

[a]The intercalation compound was dispersed in liquid ammonia at −75 °C, and the reaction mixture was quenched with D_2O.

The TG profile of the final product $\mathbf{G_{1:4}A_D(NH_3)}$ exhibits a drastically reduced mass loss in the temperature region from 100 to 350 °C in comparison to $\mathbf{G_{1:4}A_D}$, indicative for the absence of an encapsulated species (Figure S3). In addition, the maximum ion current for the mass trace m/z 2 is detected at 450 °C. Because of deuterium/hydrogen exchange reactions, no mass traces with m/z 3 or 4 were detected. Moreover, we could demonstrate the influence of the solvent by reproducing the experiment of Schlögl et al.[14] Therefore, D_2O was added to $\mathbf{G_{1:8}}$ in the total absence of any GIC exfoliating solvent. Here, a mass loss of <1% is detected in the temperature region B between 380 and 600 °C (Figure 2c,d), and a small extent of deuteration (m/z 3 and 4 max at 550 °C) can be verified by MS analysis.

The predominant sample mass loss (2.4%) takes place in the temperature region A (200−380 °C) where the mass traces m/z 19 and 20 can be attributed to HDO and D_2O. The increased detachment temperature for the m/z 3 and 4 fragments (550 °C vs 450 °C) in the case of $\mathbf{G_{1:4}A_D}$ might be explained by a predominant edge functionalization due to an inefficient exfoliation of the charged GICs. In addition, the formation of HDO probably is based on the presence of partially encapsulated KOD which cannot be removed by washing and drying during the work-up (reference experiment with KOH; see Figure S4). These encapsulation scenario is in accordance with the findings of Schlögl et al.[14] The results of our reference experiments clearly underline the importance of the proper solvent for the reductive hydrogenation/deuteration of graphene and its influence on the underlying reaction mechanism.

In the next step we studied the impact of the potassium concentration on the hydrogenation efficiency. In the case of the reductive phenylation of graphene we have already demonstrated that the degree of reduction determines the degree of covalent addend binding.[9,16] As outlined in Scheme 1, we varied the amount of potassium (K:C = 1:4, 1:8, and 1:24) while using MeOD as deuteration source. The TG-MS data (Figure 2e,f) for $\mathbf{G_{1:8}B_D}$ and $\mathbf{G_{1:4}B_D}$ demonstrate an increase of the detected mass loss from 4.9% (0.125 equiv K/C, degree of deuteration: 34.8%, $(C_1D_{0.3})_n$) to 6.1% (degree of deuteration: 48.5%, $(C_1D_{0.5})_n$) for 0.25 equiv K/C and a simultaneous ion current intensity increase for m/z 4 (D_2) from 8.9 to 12 pA, whereas the decrease of potassium to 0.04 equiv per carbon reduces the amount of deuteration to 5% ($(C_1D_{0.1})_n$) (Figure 2e,f, Figures S5−S7, and Table ST4). The results for the analogously hydrogenated samples are summarized in Figures S8−S10. Thus, the observed decrease in hydrogenation with decreasing amount of potassium underlines the above-mentioned hypoth-

DOI: 10.1021/jacs.5b11994
J. Am. Chem. Soc. 2016, 138, 1647−1652

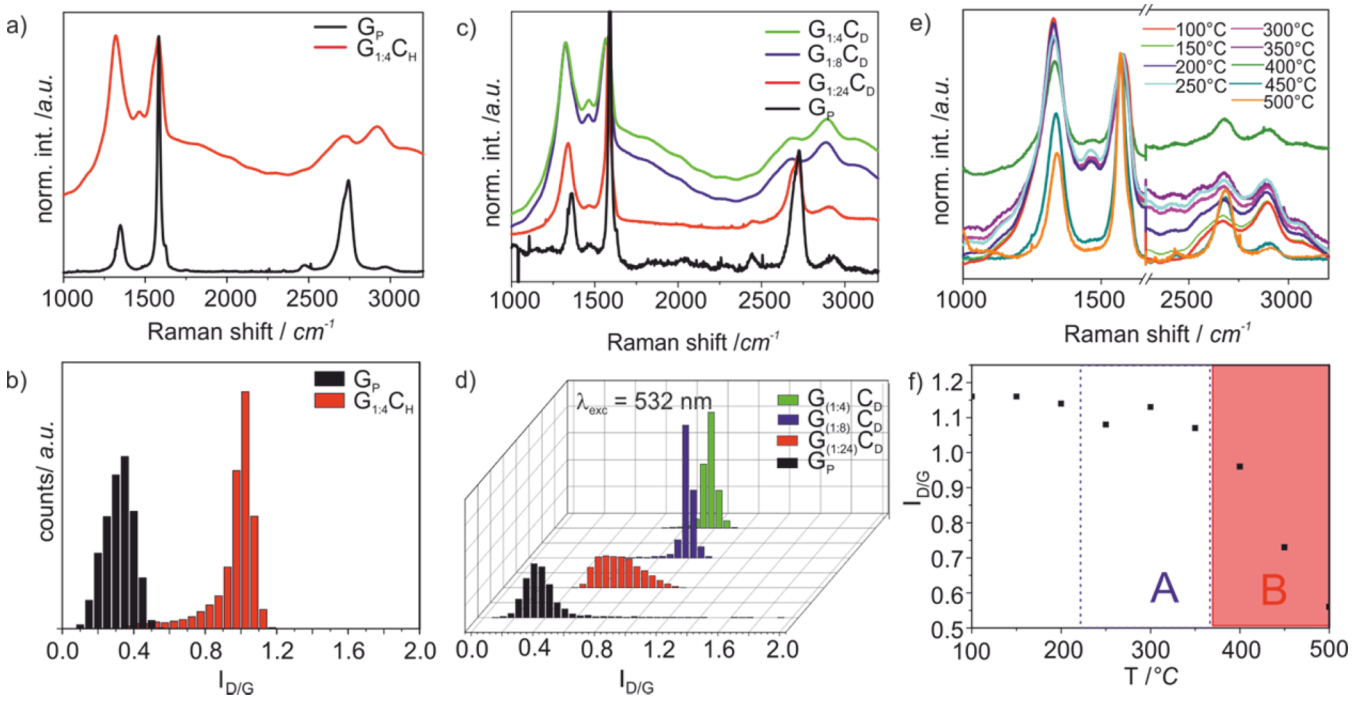

Figure 3. Statistical Raman analysis of hydrogenated and deuterated graphene. (a) Raman mean spectrum of $\mathbf{G_P}$ and $\mathbf{G_{1:4}C_H}$. (b) Statistical distribution (10.000 single point spectra) of the $I_{D/G}$ intensity ratio of the pristine starting material $\mathbf{G_P}$ (black) and the functionalized bulk material $\mathbf{G_{1:4}C_H}$ (red). (c) Raman mean spectrum of $\mathbf{G_P}$, $\mathbf{G_{1:4}C_D}$, $\mathbf{G_{1:8}C_D}$, and $\mathbf{G_{1:24}C_D}$. (d) Statistical distribution (10.000 single point spectra) of the $I_{D/G}$ intensity ratio of the pristine starting material $\mathbf{G_P}$ (black) and the functionalized bulk material $\mathbf{G_{1:4}C_D}$ (green), $\mathbf{G_{1:8}C_D}$ (blue), and $\mathbf{G_{1:24}C_D}$ (red). (e) Mean Raman spectra of $\mathbf{G_{1:4}B_D}$ at 100−500 °C. (f) $I_{D/G}$ ratio of $\mathbf{G_{1:4}B_D}$ at 100−500 °C with region A (dashed blue) and region B (red).

esis that the elemental potassium is crucial for the reaction mechanism and the final hydrogenation degree. In contrast to the Birch reduction our reductive hydrogenation delivers a way to controllably fine-tune the hydrogenation degree via adjusting the potassium amount and proton source.

Taking into account that for graphane—fully hydrogenated graphene—a maximum mass loss of 7.7% (degree of hydrogenation: 100%, $(C_1H_1)_n$) can be expected, our obtained 4.8% (degree of hydrogenation: 66.4%, $(C_1H_{0.7})_n$) in the case of the SGN_{18} (synthetic spherical graphite) starting GIC, with 0.25 equiv potassium, represents a very promising starting point for future graphane-based applications.

In addition, it can be expected—and it has been shown[9,10]—that the type of graphite, used as starting material in reductive functionalization sequences, has an impact on the final degree of functionalization. In order to investigate the basic influence of the morphology of the starting graphite, we used a natural flake graphite (NG) and an expanded powder graphite (PEX10) in addition to the synthetic spherical graphite SGN18 in the course of the reductive deuteration with *t*-BuOD as trapping reagent.

In the case of the powder graphite (3−5 μm flake size) the respective TG profile of $\mathbf{G_{1:4}C_D(PEX)}$ (Figure S11) exhibits only one region of mass loss between 300 and 500 °C (m/z 2, 3, and 4 detected by MS). Interestingly, the smaller flake size efficiently inhibits the encapsulation of THF or potassium hydroxide,[9] whereas a bigger flake size of 1000 μm as present in the natural graphite leads to the opposite effect (increase of mass loss region A) and a less effective deuteration—3.6% mass loss in region B for $\mathbf{G_{1:4}C_D(PEX)}$ (degree of deuteration: 26.4%, $(C_1D_{0.3})_n$) vs 3.1% mass loss for $\mathbf{G_{1:4}C_D(NG)}$ (degree of deuteration: 26.6%, $(C_1D_{0.3})_n$) (Figure S11 and Table ST5). As a consequence, it can be clearly seen that the hydrogenation of graphene can be influenced by the nature of the hydrogen/deuterium source, the nature of the starting material, and the amount of intercalated potassium. The resulting material can reach a maximum of 4.8% hydrogen mass loss and a maximum degree of hydrogenation of 66.4% (6.1% deuterium mass loss, degree of deuteration: 48.5%) and is in comparison to the polyhydrogenated graphene, conducting and nonfluorescent, which can be attributed to a different hydrogenation pattern.

Further unambiguous proof for the successful hydrogenation/deuteration of graphene was provided by a detailed Raman spectroscopic characterization including statistical Raman spectroscopy (SRS) and statistical Raman microscopy (SRM).[11] In general, the Raman spectrum of graphene exhibits three main peaks: the defect induced D-band at 1350 cm^{-1}, the G-band at 1582 cm^{-1}, which is characteristic for the graphitic sp^2-carbon lattice, and the 2D-band at 2700 cm^{-1} providing information about the stacking or electronic individualization of the graphene layers.[17,18] The amount of basal plane sp^3-carbon atoms, bearing a hydrogen/deuterium addend, correlates with the $I_{D/G}$ intensity ratio in the Raman spectra and therefore corresponds to the degree of functionalization[11,19,20] In Figure 3a, the Raman spectrum of the highly hydrogenated sample $\mathbf{G_{1:4}C_H}$ is presented as an example.

The statistical Raman analysis reveals a comparatively narrow distribution of basal plane sp^3-centers in the functionalized bulk material $\mathbf{G_{1:4}C_H}$, which is indicative for a highly homogeneously functionalized bulk material. A mean $I_{D/G}$ ratio of 1.0 (Figure 3b) together with a very broad D- and G-band and a fluorescence background is indicative for a covalently functionalized graphene derivative with a very high degree of functionalization. We have recently obtained similar data for hydrogenated graphene prepared under classical Birch conditions.[5] All these characteristic features can be taken as a clear indication for the introduction of an extensive amount of sp^3-

DOI: 10.1021/jacs.5b11994
J. Am. Chem. Soc. 2016, 138, 1647−1652

lattice carbon atoms carrying the covalently bound addends.[5,11] An important conclusion which can be drawn from the results of the in-depth Raman characterization of the hydrogenated and deuterated samples is that the reductive protonation/deuteration of intermediately generated graphenides yields covalently functionalized bulk materials with identical $I_{D/G}$ ratios ($\mathbf{G_{1:4}C_H}$ = 1.0, $\mathbf{G_{1:4}C_D}$ = 1.0; Figure 3b and Figure 3d, respectively). Furthermore, the nature of the starting graphite (SGN18, NG, PEX10) has no pronounced effect on the final $I_{D/G}$ ratio (Figure S12), even though the pristine graphites exhibited different defect densities. In consistency with the TG-MS results, it turns out that the main parameter which allows for a fine-tuning of the degree of functionalization is the potassium concentration used in the respective GIC starting materials. This is clarified in the following section for the reductive deuteration of SGN18 ($\mathbf{G_{1:}}_n$)—the complete data set deuteration/hydrogenation is presented in Figures S13–S18.

In the deuterated samples the mean $I_{D/G}$ ratio (Figure 3c,d) for $\mathbf{G_{1:4}A_D}$ is only slightly smaller (0.9) than the mean $I_{D/G}$ ratios of $\mathbf{G_{1:4}B_D}$ and $\mathbf{G_{1:4}C_D}$ (1.0)—again, no significant influence of the nature of the starting graphite is observed. Samples with the lowest potassium concentration in the starting GIC ($\mathbf{G_{1:24}A}$-$\mathbf{C}$) yield the lowest $I_{D/G}$ intensity ratio (0.7), whereas for $\mathbf{G_{1:8}A_D}$-$\mathbf{C_D}$ an intermediate $I_{D/G}$ ratio of 0.9 is detected. Moreover, the potassium concentration has also a direct influence on the homogeneity of the final material (Figure 3d and Figures S13–S18). Here, in both cases of reductive deuteration/hydrogenation all samples with $\mathbf{G_{1:24}}$ potassium concentration yield a remarkably broadened $I_{D/G}$ ratio distribution, indicative for an inhomogeneously functionalized bulk material.

In analogy to the TG-MS experiments, the thermal cleavage of the hydrogen and deuterium addends can be directly monitored by Raman spectroscopy. For this purpose $\mathbf{G_{1:4}B_D}$ was heated under an N_2 atmosphere from 100 to 500 °C, and every 50 °C step a Raman map of 1000 spectra was recorded. As presented in Figure 3e, the mean spectra reveal a decreasing D-band intensity with increasing temperature.

Significantly, the plot of the $I_{D/G}$ values as a function of the temperature (Figure 3f) represents exactly the same trend as the corresponding TG profile. Consistently, a pronounced decrease of the detected $I_{D/G}$ band intensity is only observed at temperatures higher than 350 °C (region B). This observation is in full agreement with the detected mass loss and recorded mass traces of H/D in the temperature region B (from 350 to 500 °C) and an unequivocal proof for covalently bound hydrogen/deuterium atoms.

The sample characterization presented so far was primarily based on the analysis of the bulk material. Here, we were able to demonstrate that an efficient bulk hydrogenation is possible on the basis of potassium intercalated graphite as starting material. That this reductive reaction protocol indeed leads to functionalized monolayer and few-layer graphene can be shown by a detailed investigation of drop-casted samples of the reaction mixture of $\mathbf{G_{1:4}C_D(NG)}$. In Figure 4 two characteristic SRM images of deuterated graphene flakes (denoted with 1 and 2) are presented.

A remarkable observation is that the spectral data of the single flakes also confirm the results of the bulk measurement with respect to the obtained degree of functionalization ($I_{D/G}$ of 1.0 and a broadened D-band). Moreover, it clearly proves the successful production of a deuterated monolayer (flake 1) and few-layer graphene (flake 2) with a respective $I_{2D/G}$ ratio between 3.0 and 1.0 and a 2D-band FWHM of 30 cm^{-1} for flake 1 and 59 cm^{-1} for flake 2.

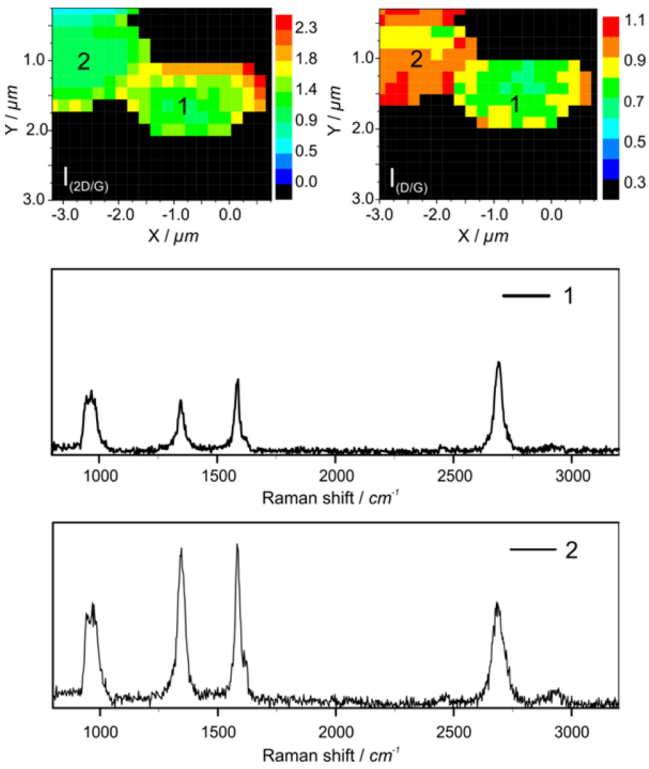

Figure 4. Top: SRM image of $\mathbf{G_{1:4}C_D(NG)}$ flake 1 and 2: (left) plot of the $I_{2D/G}$ intensity ratio; (right) plot of the $I_{D/G}$ intensity ratio. Bottom: Raman single-point spectra of flake 1 and flake 2.

CONCLUSION

In conclusion, we presented an efficient protocol for the reductive hydrogenation/deuteration of potassium intercalated graphite as starting material. In this way, a highly hydrogenated bulk material (4.8% mass loss of hydrogen; 7.7% theoretical value for graphane) is accessible. The successful synthesis has been proven by detailed TG-MS and Raman spectroscopic investigations. The variation of the graphite starting material, hydrogen/deuterium source, and potassium concentration showed that these parameters have a distinct influence on the hydrogen content in the final material.

By the right combination of these parameters, a tunable degree of functionalization can be accomplished. In addition, the covalent binding of hydrogen is reversible, and the attached hydrogen atoms can thermally be detached in a temperature region between 350 and 600 °C. As concluded from SRS and SRM, the reductive hydrogenation yields a functionalized bulk material mainly consisting of hydrogenated monolayer and few-layer graphene.

ASSOCIATED CONTENT

Supporting Information

The Supporting Information is available free of charge on the ACS Publications website at DOI: 10.1021/jacs.5b11994.

Experimental details regarding the reductive hydrogenation/deuteration of the different graphite starting materials; additional TG-MS data and Raman analysis (PDF)

DOI: 10.1021/jacs.5b11994
J. Am. Chem. Soc. 2016, 138, 1647–1652

AUTHOR INFORMATION

Corresponding Author

*E-mail: andreas.hirsch@fau.de (A.H.).

Notes

The authors declare no competing financial interest.

ACKNOWLEDGMENTS

The authors thank the Deutsche Forschungsgemeinschaft (DFG-SFB 953, Project A1 "Synthetic Carbon Allotropes") for financial support. The research leading to these results has received partial funding from the European Union Seventh Framework Programme under grant agreement no. 604391 Graphene Flagship.

REFERENCES

(1) Pumera, M.; Wong, C. H. A. *Chem. Soc. Rev.* **2013**, *42*, 5987.
(2) Sofo, J. O.; Chaudhari, A. S.; Barber, G. D. *Phys. Rev.* **2007**, *75*, 153401.
(3) Elias, D. C.; Nair, R. R.; Mohiuddin, T. M. G.; Morozov, S. V.; Blake, P.; Halsall, M. P.; Ferrari, A. C.; Boukhvalov, D. W.; Katsnelson, M. I.; Geim, A. K.; Novoselov, K. S. *Science* **2009**, *323*, 610.
(4) Yang, Z.; Sun, Y.; Alemany, L. B.; Narayanan, T. N.; Billups, W. E. *J. Am. Chem. Soc.* **2012**, *134*, 18689.
(5) Schäfer, R. A.; Englert, J. M.; Wehrfritz, P.; Bauer, W.; Hauke, F.; Seyller, T.; Hirsch, A. *Angew. Chem., Int. Ed.* **2013**, *52*, 754.
(6) Birch, A. J. *J. Chem. Soc.* **1944**, 430.
(7) Strauss, V.; Schäfer, R. A.; Hauke, F.; Hirsch, A.; Guldi, D. M. *J. Am. Chem. Soc.* **2015**, *137*, 13079.
(8) Englert, J. M.; Dotzer, C.; Yang, G.; Schmid, M.; Papp, C.; Gottfried, J. M.; Steinrück, H.-P.; Spiecker, E.; Hauke, F.; Hirsch, A. *Nat. Chem.* **2011**, *3*, 279.
(9) Hof, F.; Schäfer, R. A.; Weiss, C.; Hauke, F.; Hirsch, A. *Chem.—Eur. J.* **2014**, *20*, 16644.
(10) Knirsch, K. C.; Englert, J. M.; Dotzer, C.; Hauke, F.; Hirsch, A. *Chem. Commun.* **2013**, *49*, 10811.
(11) Englert, J. M.; Vecera, P.; Knirsch, K. C.; Schäfer, R. A.; Hauke, F.; Hirsch, A. *ACS Nano* **2013**, *7*, 5472.
(12) Viculis, L. M.; Mack, J. J.; Kaner, R. B. *Science* **2003**, *299*, 1361.
(13) Bergbreiter, D. E.; Killough, J. M. *J. Am. Chem. Soc.* **1978**, *100*, 2126.
(14) Schlögl, R.; Boehm, H. P. *Carbon* **1984**, *22*, 351.
(15) Ebert, L. B.; Mills, D. R.; Scanlon, J. C. *Solid State Ionics* **1986**, *22*, 143.
(16) Vecera, P.; Edelthalhammer, K.; Hauke, F.; Hirsch, A. *Phys. Stat. Solidi B* **2014**, *251*, 2536.
(17) Ferrari, A. C.; Basko, D. M. *Nat. Nanotechnol.* **2013**, *8*, 235.
(18) Malard, L. M.; Pimenta, M. A.; Dresselhaus, G.; Dresselhaus, M. S. *Phys. Rep.* **2009**, *473*, 51.
(19) Lucchese, M. M.; Stavale, F.; Ferreira, E. H. M.; Vilani, C.; Moutinho, M. V. O.; Capaz, R. B.; Achete, C. A.; Jorio, A. *Carbon* **2010**, *48*, 1592.
(20) Cançado, L. G.; Jorio, A.; Ferreira, E. H. M.; Stavale, F.; Achete, C. A.; Capaz, R. B.; Moutinho, M. V. O.; Lombardo, A.; Kulmala, T. S.; Ferrari, A. C. *Nano Lett.* **2011**, *11*, 3190.

DOI: 10.1021/jacs.5b11994
J. Am. Chem. Soc. 2016, 138, 1647−1652